DRAG FORCES OVER THE SOLAR PANELS BY COMPUTATIONAL FLUID DYNAMICS

Panga Surendra Reddy

Lecturer in Physics
Department of Technical Education, Government Polytechnic Proddatur.

Abstract:
"This study investigates the aerodynamic drag forces acting on solar panel installations, a crucial consideration for their structural integrity and long-term performance. Wind loads can exert significant stress on solar panels, potentially leading to damage or failure. This research examines the factors influencing drag forces, including panel inclination, array configuration, wind speed, and environmental conditions. Utilizing computational fluid dynamics (CFD) and/or wind tunnel testing, this analysis quantifies the drag coefficients and force distributions across various solar panel arrangements. The findings provide valuable insights for optimizing solar panel design and installation practices, ensuring their resilience against wind-induced loads and enhancing the reliability of solar energy systems."

Keywords: CFD (Computational Fluid Dynamics), Drag Force, Solar Panels.

1. INTRODUCTION:

"The global shift towards renewable energy sources has propelled solar photovoltaic (PV) systems to the forefront of power generation. Solar installations proliferate across diverse geographical locations, ensuring their structural integrity against environmental stressors becomes paramount. [2] Among these stressors, wind loads pose a significant threat, potentially leading to panel damage, system failure, and substantial economic losses. [3] The aerodynamic drag forces exerted by wind on solar panels are critical parameters in the structural design and performance assessment of these systems. [4] Unlike static loads, wind forces are dynamic and complex, varying with wind speed, direction, panel inclination, array configuration, and surrounding terrain. [5] Accurate quantification and analysis of these drag forces are essential for developing robust and reliable solar panel installations. This research aims to address the critical need for a comprehensive understanding of drag forces on solar panels, providing valuable insights for optimizing design practices and enhancing the long-term performance and resilience of solar energy systems. By investigating the influence of key parameters on drag coefficients and force distributions, this study seeks to contribute to the development of safer and more efficient solar energy technologies."

1.2 METHODOLOGY: This study employs ANSYS Fluent, widely recognized CFD software, to investigate the aerodynamic drag forces acting on solar panels under various wind conditions. The methodology is structured as follows:

1.21 Geometry Creation

A 3D model of the solar panel and its supporting structure is created using ANSYS Design Modeler or compatible CAD software. The model includes accurate representations of the panel's dimensions, inclination angle, and surface features. The surrounding air domain is defined as a rectangular or hemispherical enclosure, sufficiently large to minimize boundary effects on the flow field. For array studies, multiple panels with accurate spacing and row configurations are modeled.

1.22 Meshing

The computational domain is discredited into a finite number of control volumes using ANSYS Meshing. A structured or unstructured mesh is generated, with finer mesh resolution in regions of high flow gradients, such as near the panel surfaces and in the wake region. Boundary layer meshing is implemented to accurately capture the viscous effects near the panel surface. Mesh independence studies are conducted to ensure that the numerical results are independent of the mesh resolution. This involves refining the mesh until the drag coefficient converges to a stable value.

1.23 Solver Setup in ANSYS Fluent

The appropriate turbulence model is selected based on the Reynolds number and the complexity of the flow. Common choices include the k-epsilon (realizable or standard) or k-omega SST models. The steady-state or transient solver is chosen based on the nature of the flow. For most drag force studies steady state analysis is sufficient.

1.24 Boundary conditions are defined

Inlet: Uniform velocity profile with specified wind speed and direction.
Outlet: Pressure outlet with zero gauge pressure.
Walls: No-slip boundary condition for the solar panel and supporting structure.
Symmetry planes: where appropriate.

The SIMPLE or COUPLED algorithm is used for pressure-velocity coupling.

Second-order discretization schemes are employed for momentum and turbulence equations to enhance accuracy. Convergence criteria are defined for residuals and drag force monitoring.

1.25 Simulation Execution

The simulation is executed in ANSYS Fluent, and the solution is monitored for convergence. The drag force and drag coefficient are calculated and recorded. The simulation is run for multiple wind speeds and angles of attack to assess the impact of these parameters on drag.

1.26 Post-Processing and Data Analysis

The simulation results are visualized using ANSYS CFD-Post to analyze the flow field, pressure distribution, and velocity vectors The drag coefficient is calculated using the formula:

$c_d = \rho u^2 A^2 F_d$

Where:

$C_d$is the drag coefficient.
$F_d$is the drag force.
ρ is the air density.
U is the wind speed.
A is the reference area of the solar panel.

The distribution of drag force across the panel surface is analyzed. Graphical representations of the results are created to show the relationship between drag coefficient, wind speed, and panel inclination. For array studies, the effect of panel spacing and row configuration on drag is analyzed.

1.27 Validation

If possible, the CFD results are validated by comparing them with experimental data from wind tunnel tests or existing literature. This comparison helps to assess the accuracy and reliability of the CFD simulations. This methodology provides a comprehensive framework for investigating drag forces on solar panels using ANSYS CFD, enabling researchers to gain valuable insights for optimizing solar panel design and installation.

2. DRAG FORCES ON THE SOLAR PANELS

The below plots show how the drag force is acting on each panel at different time steps. The graphs are plotted between drag force and time with an AOA of 0O and velocities 5 m/s and 25 m/s. Plots 1 and 2 illustrate the time vs drag plotted for traditional panels, whereas 3 and 4 depict the time vs drag plotted for optimized panels. Each panel is indicated with a different line and can be identified using the legend provided in the plot. When the traditional panels are subjected to a velocity of 5 m/s, the drag force induced is reversed in direction with a drag magnitude of around -180N. Later as the time increases, the drag force decreases by about 50 N and 100N and is nearly constant as illustrated in plot 1. Plot 2 delineates the drag force when conventional panels are subjected to a flow rate of 25m/s. The drag force induced gradually decreased for a period of time and becomes constant. Plot 3 and 4 show drag force induced in optimized panels when they are subjected to 5 m/s and 25 m/s respectively. When the optimized panels are subjected to a flow velocity of 5 m/s, the drag force induced decreases gradually and sets to become constant throughout the time period, and the graph trend is vice versa when the panels are subjected to a flow rate of 25 m/s. In all these cases when the panels are exposed to flow velocity of 5 m/s and 25 m/s with an AOA of 0O the maximum drag is induced in the first row of panels. Table 4.6.1 presents the drag force (in Newton) comparison of ground mounted solar farm at θ= 0°.

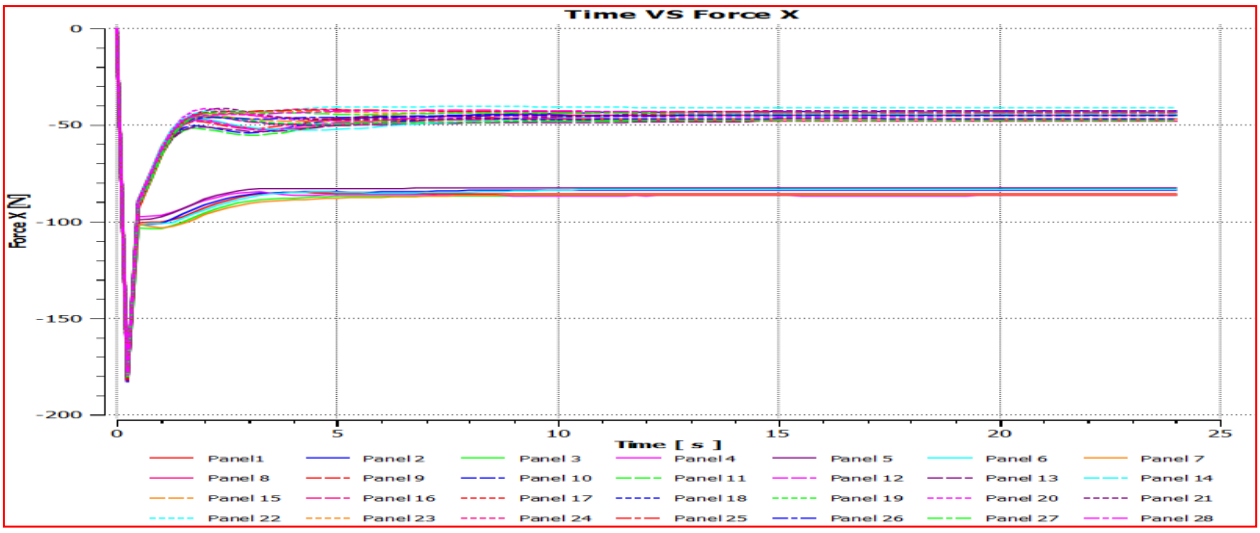

Plot. 1 Time vs drag force induced on solar panels with θ= 0°, U= 5 m/s

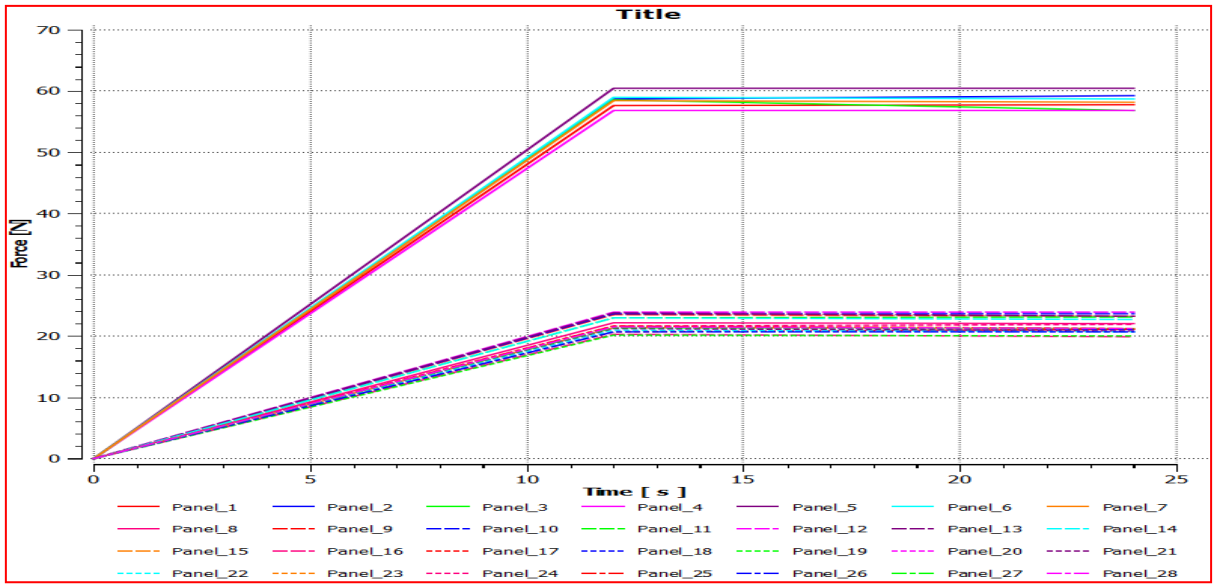

Plot. 2 Time vs drag force induced on conventional solar panels with θ= 0°, U= 25 m/s

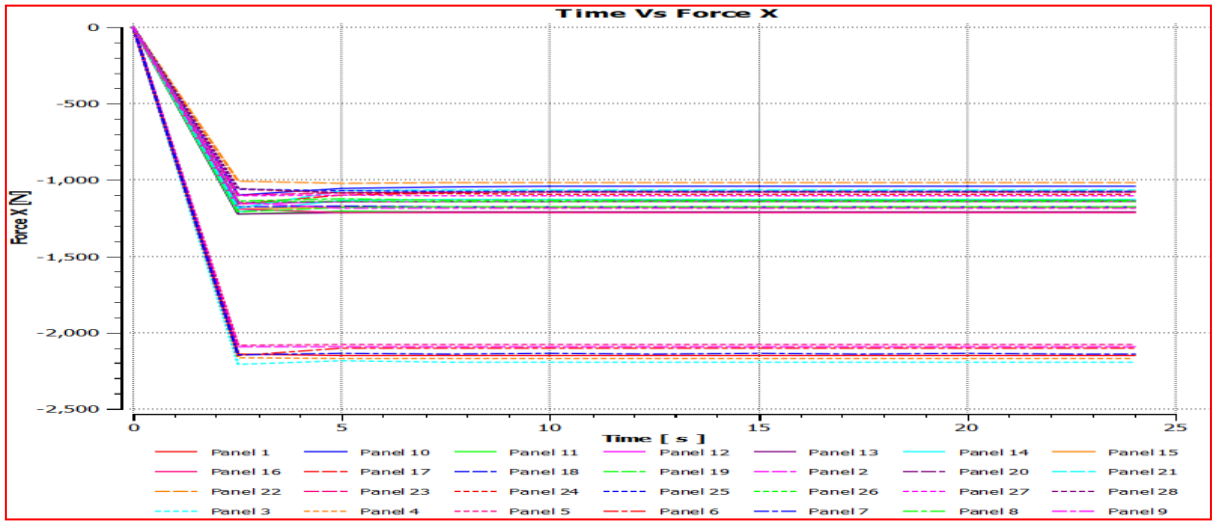

Plot. 3 Time vs drag force induced on optimized solar panels with θ= 0°, U= 5 m/s

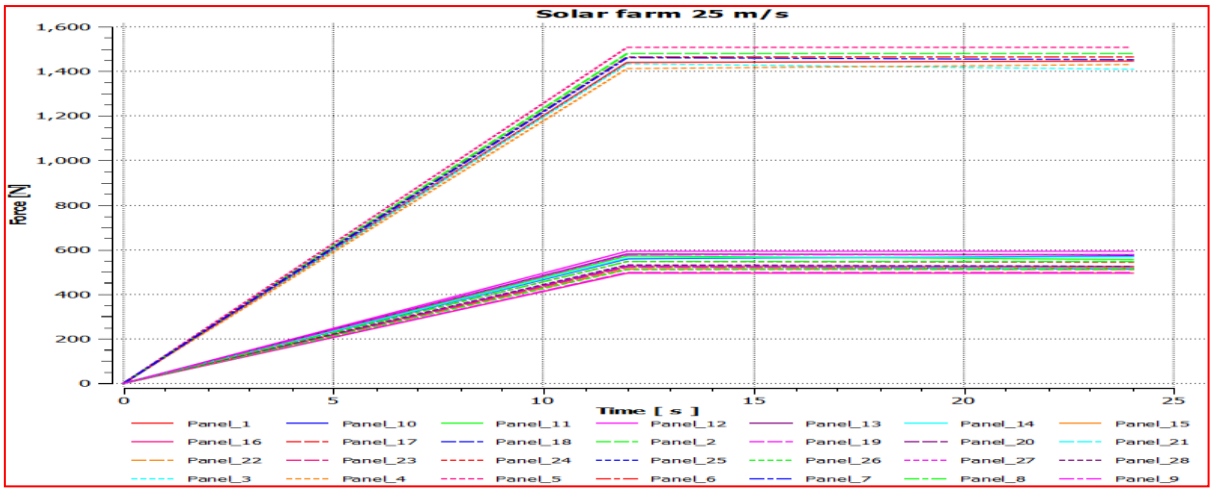

Plot. 4 Time vs drag force induced on optimized solar panels with θ= 0°, U= 25 m/s

Table 1: Drag force (Newton) comparison of ground mounted solar farm at θ= 0°

Panel No	5m/s Conventional	5m/s Optimized	25m/s Conventional	25m/s Optimized
Panel 1	180.34	57.73	2151.7	1445.62
Panel 2	182.17	59.27	2092.88	1479.42
Panel 3	179.67	58.59	2205.83	1434.23
Panel 4	182.57	56.86	2170.74	1431.33
Panel 5	181.24	60.48	2080.44	1508.07
Panel 6	181.37	58.97	2147.52	1464.62
Panel 7	181.72	58.47	2145.79	1460.66
Panel 8	181.57	22.12	1137.92	547.23
Panel 9	181.86	23.42	1183.56	576.83
Panel 10	181.72	23.68	1100	571.62
Panel 11	181.26	23.14	1222.66	572.47
Panel 12	183.42	23.95	1156.16	591.85
Panel 13	188.82	23.78	1220.54	579.86
Panel 14	180.71	22.95	1209.21	567.55
Panel 15	179.83	21.35	1189.67	526.35
Panel 16	182.44	20.33	1214.3	493.62
Panel 17	180.42	21.1	1158.3	514.42
Panel 18	178.53	21.4	1173.99	524.67
Panel 19	179.29	20.19	1207.59	496.94
Panel 20	178.53	21.28	1150.35	522.16
Panel 21	180.41	21.28	1190.51	522.16

Panel 22	173.44	20.96	1020.93	512.3
Panel 23	176.43	21.59	1100.19	523.16
Panel 24	176.36	21.87	1090.38	546.59
Panel 25	176.16	21.58	1070.18	531.33
Panel 26	176.73	20.74	1150.17	512.65
Panel 27	175.86	21.32	1100.54	527.74
Panel 28	176.38	21.5	1080.96	530.07

The plots below represent the drag force prompted on each panel at various time steps. The charts are plotted between drag force and time with an AOA of 45O and speeds of 5 m/s and 25 m/s. Plots 5 and 6 outline the time vs drag plotted for conventional panels, while 7 and 8 portray the time vs drag plotted for upgraded panels. Each panel is demonstrated with an alternate line and can be recognized with the help of legend given in the plot. At the point when the conventional panels are exposed to a speed of 5 m/s, the drag force incited in certain panels is switched in direction with a drag size of around - 250N and around - 200N for different panels. The drag forces actuated on the panels stay to vary persistently as addressed in plot 5. Plot 6 depicts the drag force when customary panels are exposed to a velocity of 25m/s. The drag force prompted diminishes step by step for a while and stays to change unpredictably. Plots 7 and 8 show drag force incited on enhanced panels when they are exposed to 5 m/s and 25 m/s each. For this situation, the pattern of forces actuated cannot be resolved as there is no consistency. In every one of these situations when the panels are presented to a wind pace of 5 m/s and 25 m/s with an AOA 45O, the greatest drag is incited in the left side panels. Table 4.6.2 presents the drag force (in Newton) comparison of ground mounted solar farm at θ= 45°.

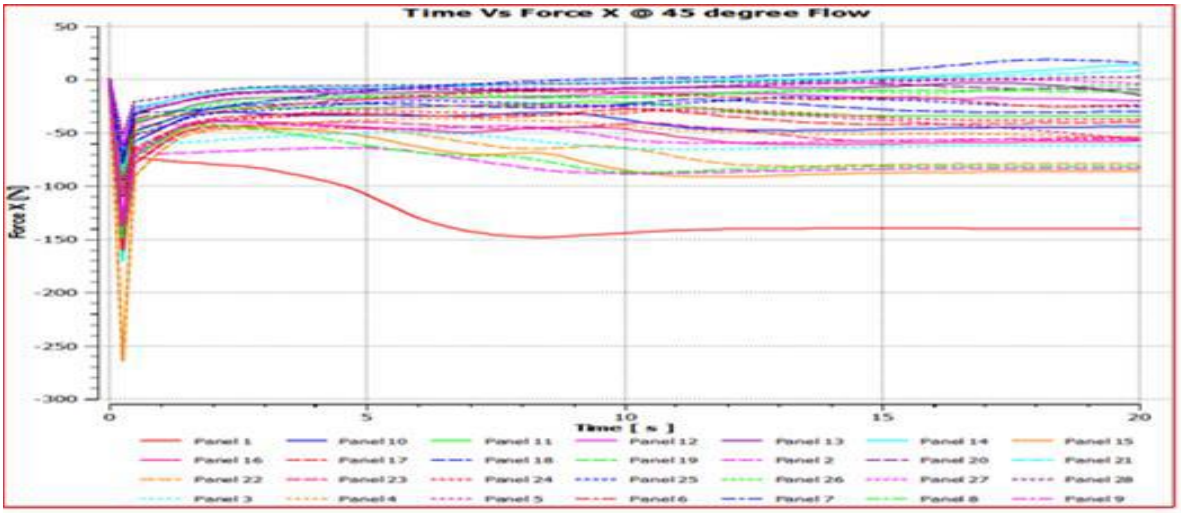

Plot. 5 Time vs drag force induced on conventional solar panels with θ=45°, U= 5 m/s

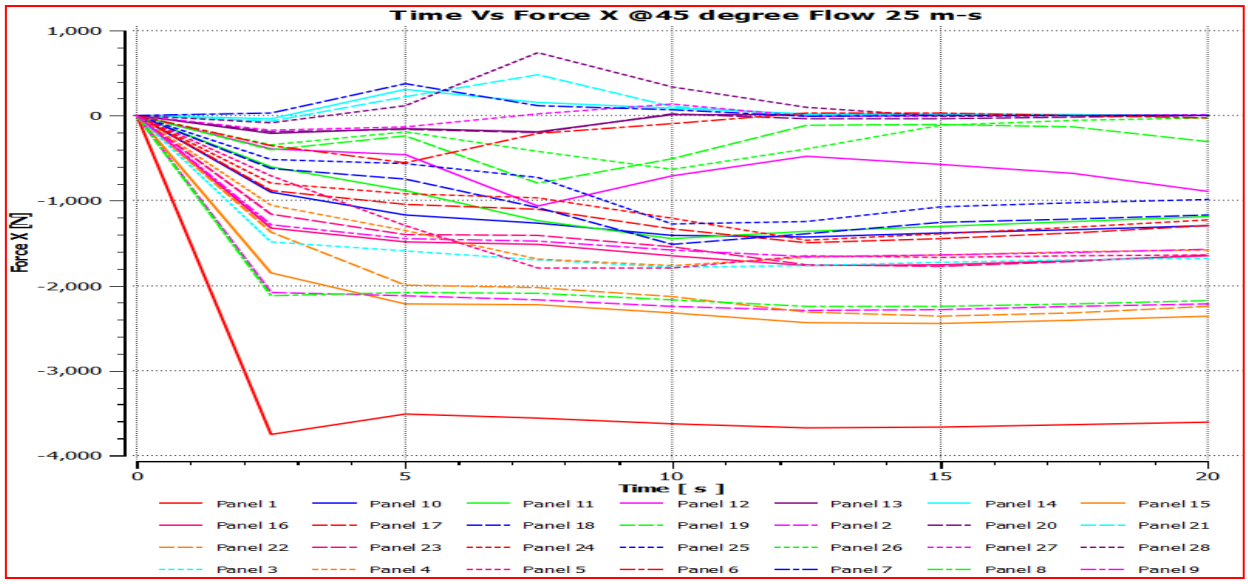

Plot. 6 Time vs drag force induced on conventional solar panels with θ=45°, U= 25 m/s

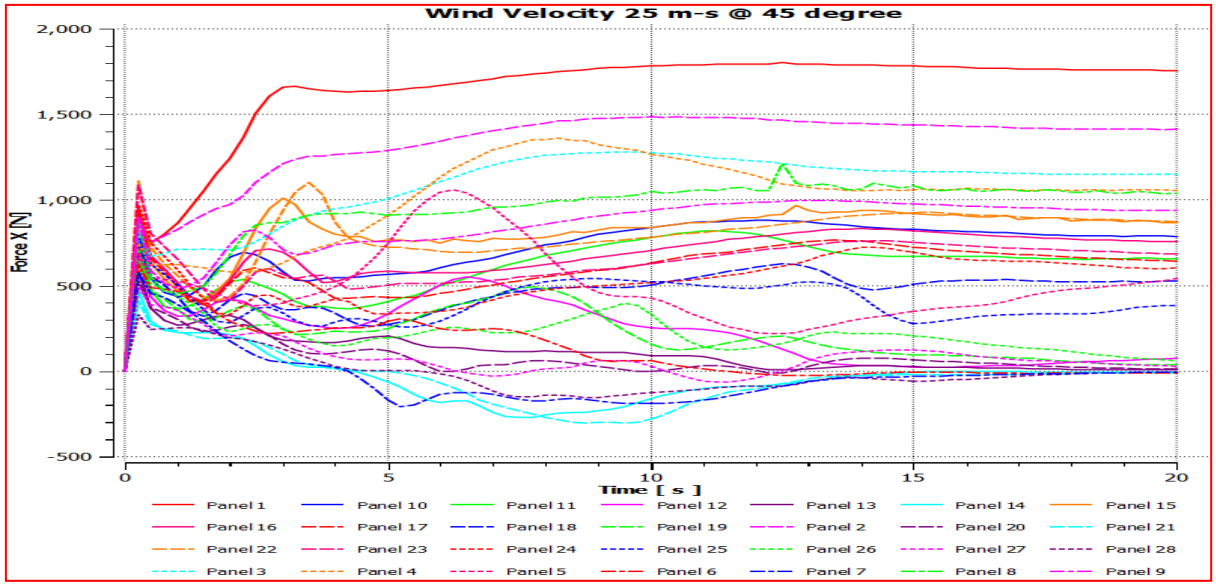

Plot.7 Time vs drag force induced on optimized solar panels with θ=45°, U= 5 m/s

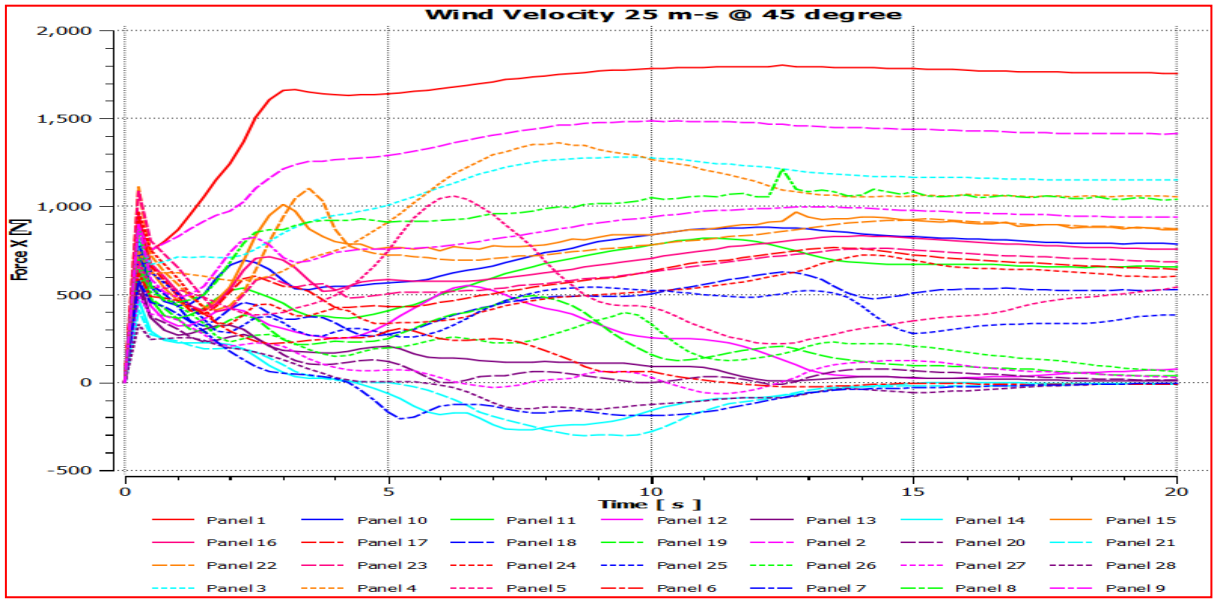

Plot. 8 Time vs drag force induced on optimized solar panels with θ=45°, U= 25 m/s

Table 2: Drag force (Newton) comparison of solar farm at θ= 45°

Panel No	5m/s Conventional	5m/s Optimized	25m/s Conventional	25m/s Optimized
Panel 1	137.38	53.395	3753.63	877.62
Panel 2	130.63	52.715	2080	883.82
Panel 3	85.98	50.985	1785.42	807.7
Panel 4	107.59	54.605	1737.64	747.77
Panel 5	62.26	53.095	1789.17	689.29
Panel 6	149.35	52.595	355.63	622.38
Panel 7	78.39	16.245	374.82	576.02
Panel 8	149.06	17.545	2246.12	885.84
Panel 9	138.24	17.805	1655.44	899.01
Panel 10	95.3	17.265	1430	807.62
Panel 11	108.29	18.075	1450	731.42
Panel 12	92.43	17.905	1070	668.75
Panel 13	140.98	17.075	214	589.75
Panel 14	170.62	15.475	311	471.2
Panel 15	159.33	14.455	2450	946.09
Panel 16	148.62	15.225	1760.28	947.2
Panel 17	159.94	15.525	1490	934.92
Panel 18	107.29	14.315	1510	745.73
Panel 19	89.58	15.405	798.65	629.73
Panel 20	73.84	15.405	191.69	527.48
Panel 21	65.83	15.085	481.43	413.91
Panel 22	264.22	15.715	2359.92	1113.87
Panel 23	157.53	15.995	1752.16	1087.05
Panel 24	161.05	15.705	1462.18	971.82
Panel 25	110.01	14.865	1274.25	795.38
Panel 26	85.11	15.445	632.22	646.14
Panel 27	63.07	15.625	172.79	491.07
Panel 28	52.77	15.725	743.33	329.19

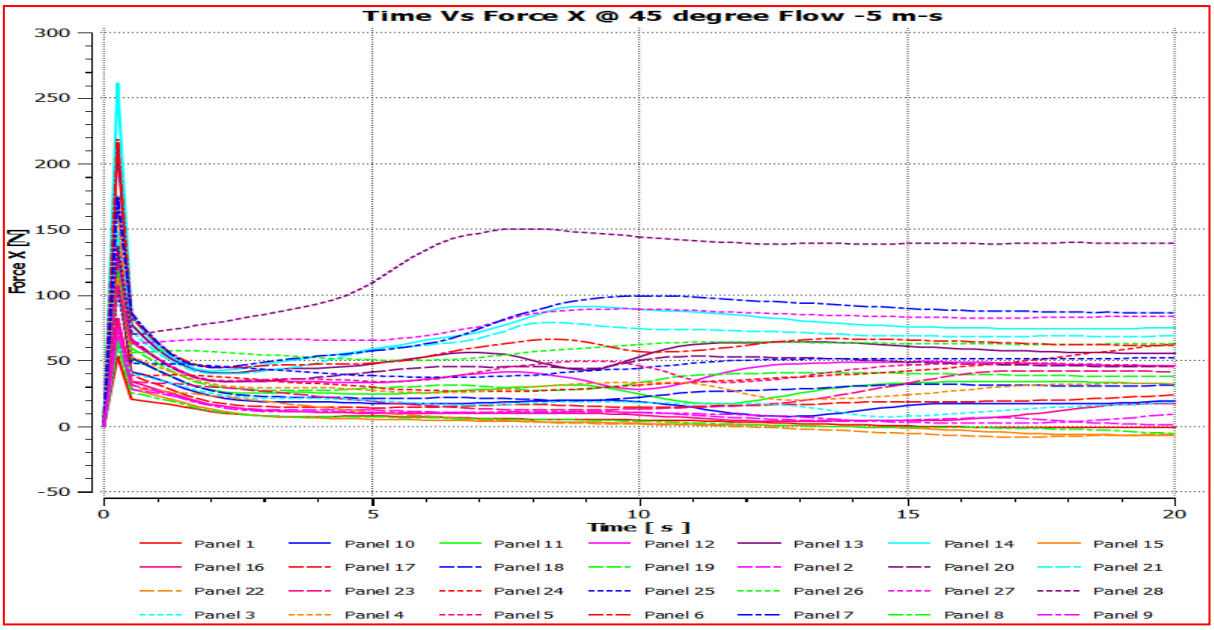

Plot. 9 Time vs drag force induced on conventional solar panels with θ=135°, U= 5 m/s

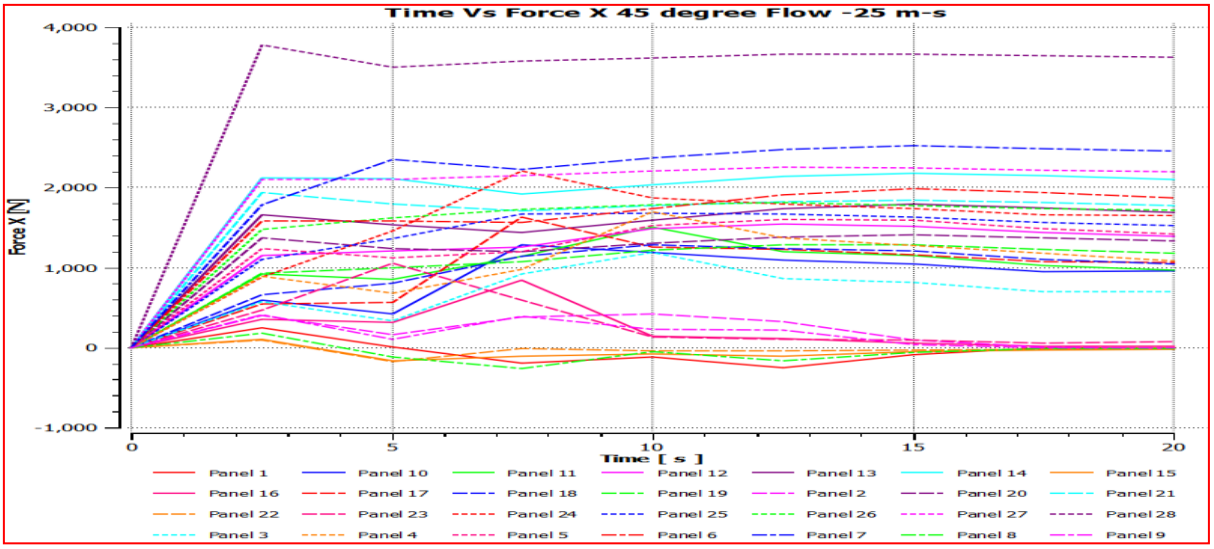

Plot. 10 Time vs drag force induced on conventional solar panels with θ=135°, U= 25 m/s

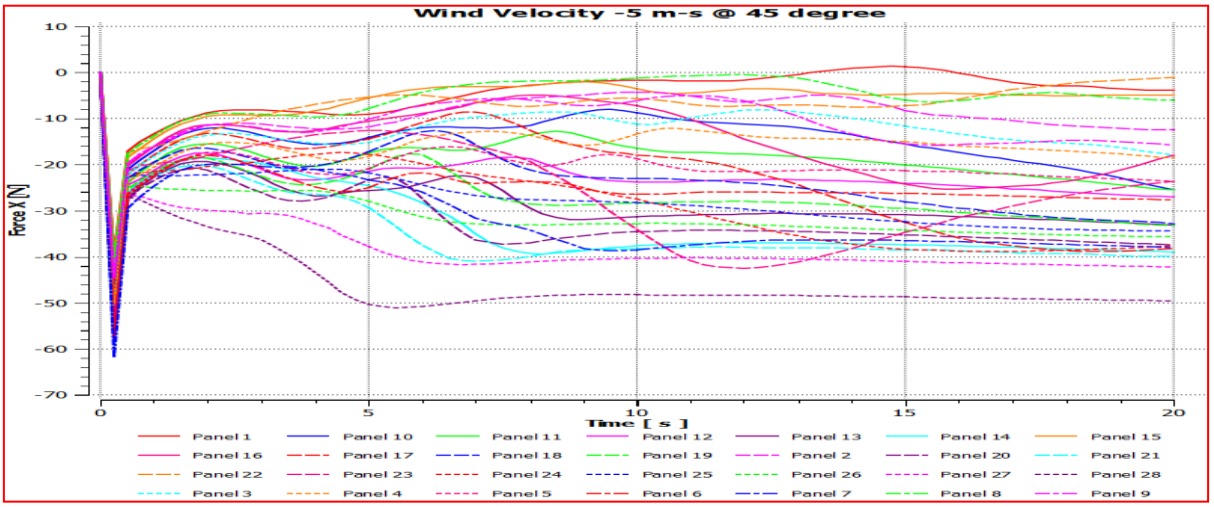

Plot. 11 Time vs drag force induced on optimised solar panels with θ=135°, U= 5 m/s

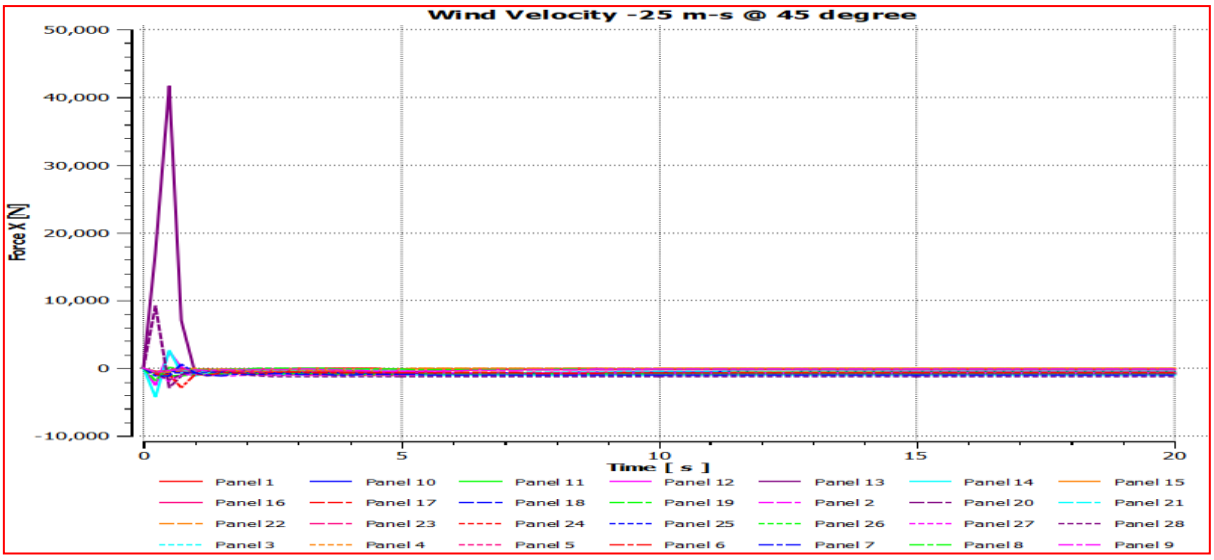

Plot. 12 Time vs drag force induced on optimized solar panels with θ=135°, U= 25 m/s

Table 3: Drag force (Newton) comparison of solar farm at θ=135˚

Panel No	5m/s Conventional	5m/s Optimized	25m/s Conventional	25m/s Optimized
Panel 1	53.41	39.28	4692.03	490.62
Panel 2	66.9	41.41	2600	569.45
Panel 3	63.87	43.9	2231.77	616.64
Panel 4	112.85	50.22	2172.05	715.07
Panel 5	107.38	57.44	2236.46	823.08
Panel 6	219.02	57.02	444.53	865.64
Panel 7	175.32	61.88	468.52	1101.94
Panel 8	63.43	40.6	2807.65	504.53
Panel 9	74.33	44.65	2069.3	547.93
Panel 10	65.69	46.14	1787.5	621.85
Panel 11	110.22	49.89	1812.5	821.77
Panel 12	131.14	53.19	1337.5	2570.13
Panel 13	215.65	57.92	267.5	1712.23
Panel 14	261.97	57.42	388.75	4262.83
Panel 15	72.28	39.88	3062.5	518.31
Panel 16	81.66	45.02	2200.35	579.2
Panel 17	119.69	50.03	1862.5	651.03
Panel 18	113.22	51.54	1887.5	739.6
Panel 19	124.46	51.81	998.31	1769.55
Panel 20	138.8	57.03	239.61	9250.44

Panel 21	148.84	54.53	601.78	918.74
Panel 22	175.73	41.07	2949.9	540.99
Panel 23	83.24	48.5	2190.2	643.4
Panel 24	122.71	46.58	1827.72	665.89
Panel 25	106.09	49.77	1592.81	692.26
Panel 26	119.38	52.89	790.27	671.42
Panel 27	133.17	53.43	215.98	739.12
Panel 28	136.81	55.64	929.16	800.12

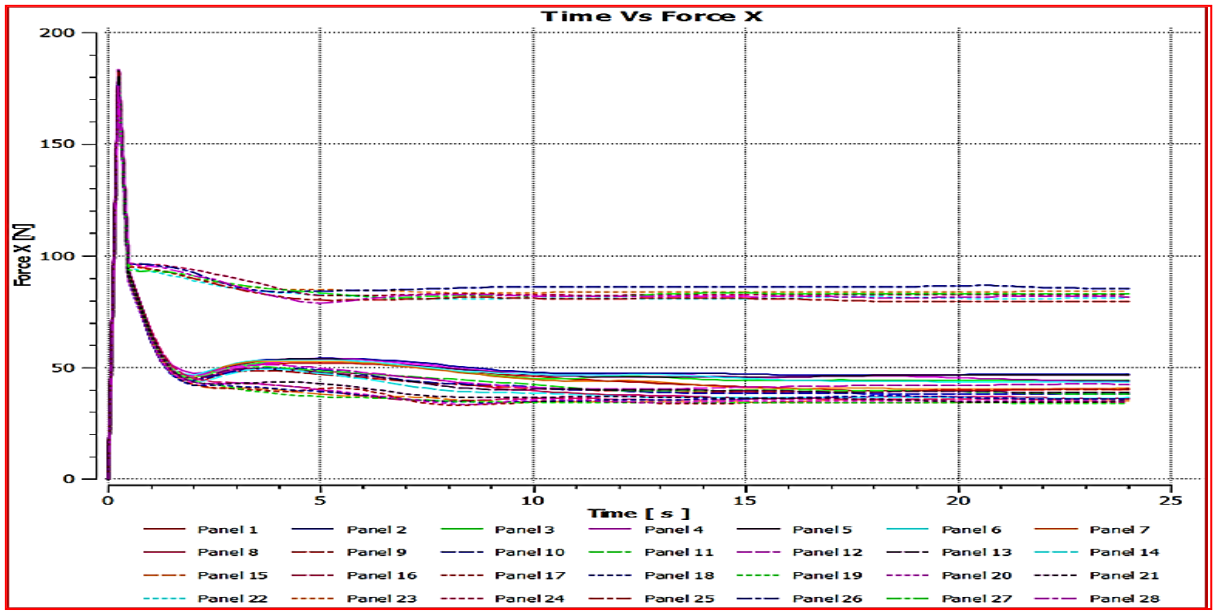

Plot. 13 Time vs drag force induced on conventional solar panels with θ=180°, U= 5m/s

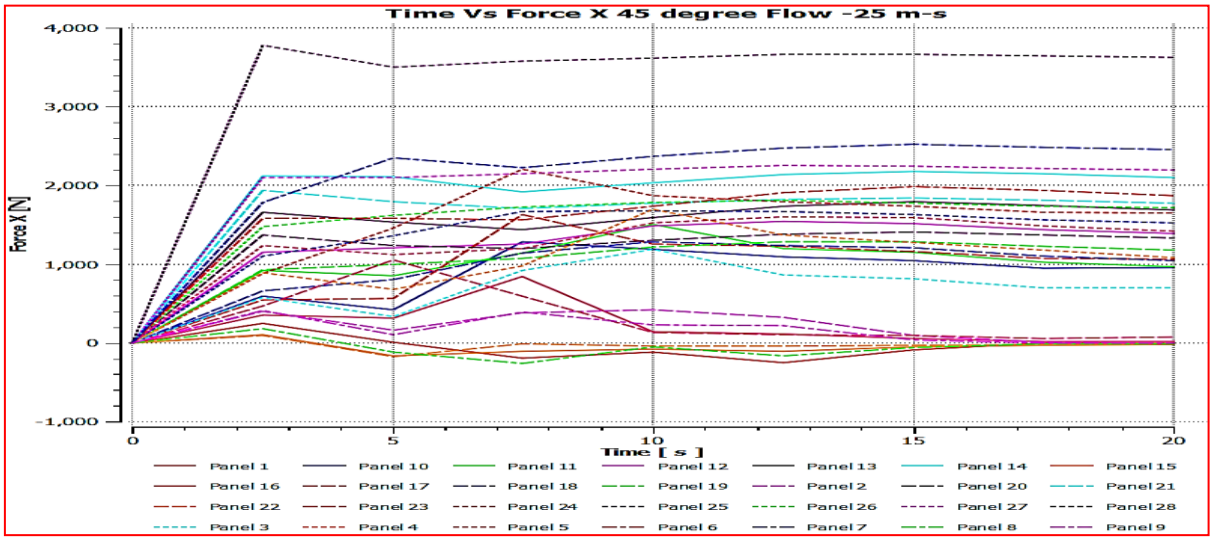

Plot. 14 Time vs drag force induced on conventional solar panels with θ=180°, U= 25 m/s

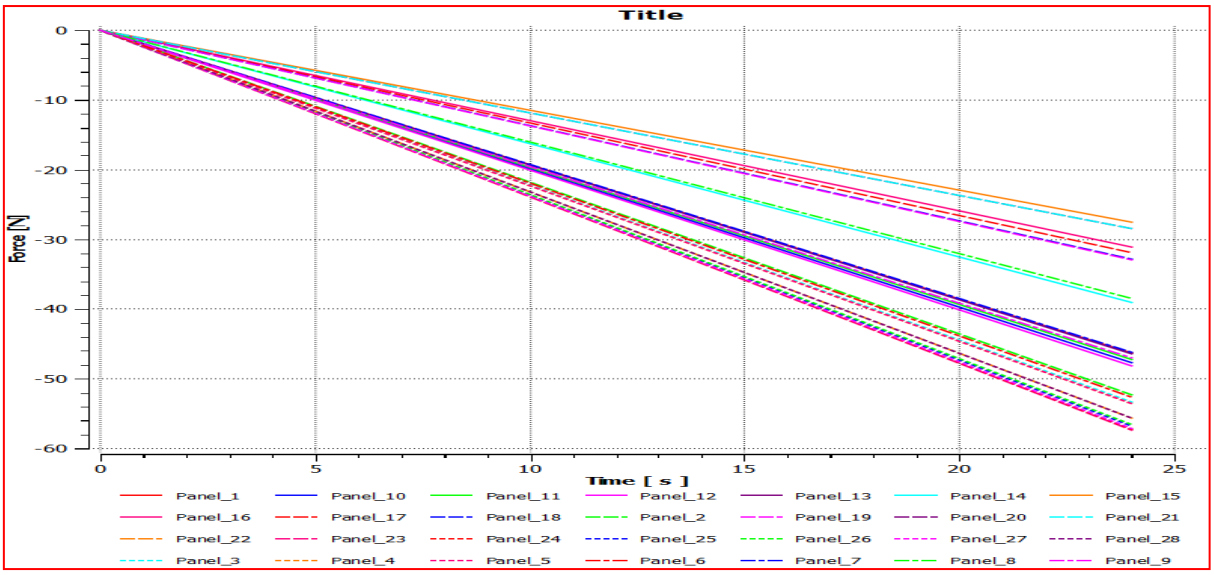

Plot. 15 Time vs drag force induced on optimized solar panels with θ=180°, U= 5 m/s

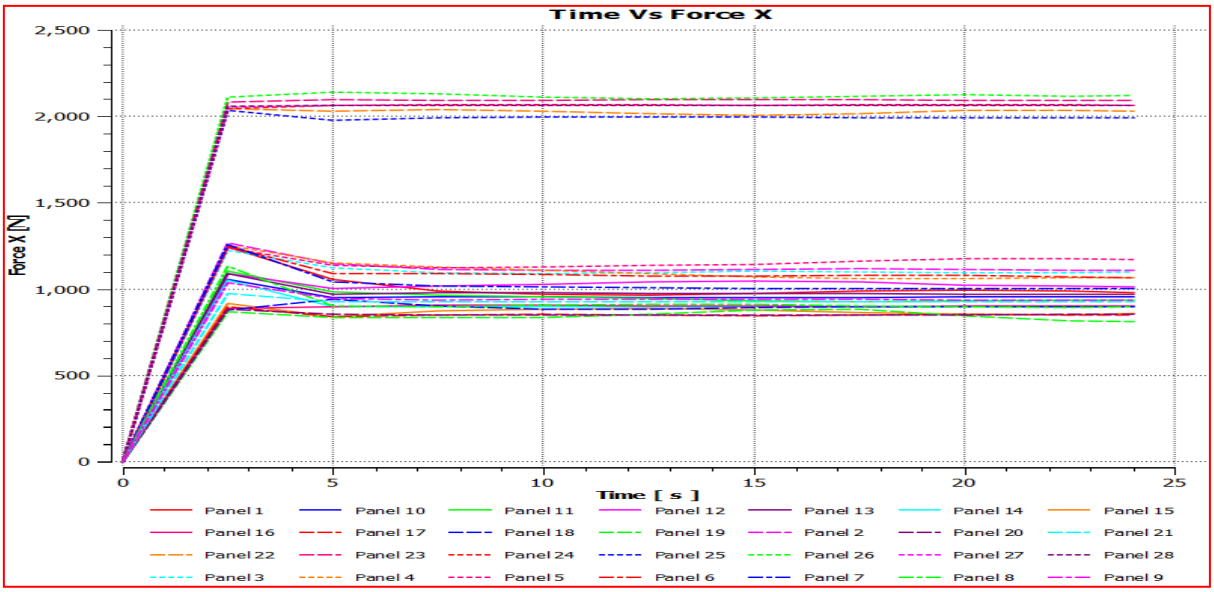

Plot. 16 Time vs drag force induced on optimized solar panels with θ=180°, U= 25 m/s

The above plots show how the drag force is circling back to each panel at different time steps. The graphs are plotted between drag force and time with an AOA of 180O and speeds 5 m/s and 25 m/s. Plots 13 and 14 outline the time vs drag plotted for regular panels, however 15 and 16 depict the time vs drag plotted for optimized panels. Each panel is shown with a substitute line and can be recognized using the legend gave in the plot. Right when the ordinary panels are presented to a speed of 5 m/s, the drag force induced is significant, i.e., 180N. Later as time grows the drag force decreased in some place in the scope of 50N and 100N anyway the forces incited in a segment of the panels stay to be in a consistent state. Plot 14 portrays the drag force when standard panels are presented to a velocity of 25m/s. The drag force actuated is logically extended for some time and will overall show up at a state of consistent. Plots 15 and 16 show drag force activated in optimized panels when they are presented to 5 m/s and 25 m/s exclusively. Right when the optimized panels are presented to a stream speed of 5 m/s the drag force started is expanded quickly to a force of 60N the opposite way and when it is presented to 25 m/s the forces impelled are altogether expanded to around 180N. In all of these circumstances when the panels are introduced to a velocity of 5 m/s and 25 m/s with an AOA of 180O, the most limit drag is induced in the last column of panels. Table 4.6.4 presents the drag force (in Newton) comparison of ground mounted solar farm at θ= 180°.

Table 4**:** Drag force (Newton) comparison of solar farm at θ=180˚

Panel No	**5m/s Conventional**	**5m/s Optimized**	**25m/s Conventional**	**25m/s Optimized**
Panel 1	176.54	46.33	1241.45	473.72
Panel 2	171.95	52.03	1265.63	530.8
Panel 3	174.20	53.35	1223.93	455.96
Panel 4	174.65	53.49	1252.8	473.4
Panel 5	174.05	53.5	1240.4	462.2
Panel 6	175.73	52.68	1246.39	487.19
Panel 7	175.26	46.12	1256.22	490.11
Panel 8	175.34	38.45	1131.27	409.63
Panel 9	178.19	47.02	1034.92	334.46
Panel 10	178.26	47.69	1056.62	1184.23
Panel 11	178.49	47.26	1105.45	1174.54
Panel 12	178.91	48.12	1090.02	1188.53
Panel 13	176.21	46.43	1091.31	1153.46
Panel 14	180.27	39.05	1052.99	963.42
Panel 15	180.71	27.49	914.7	675.15
Panel 16	180.90	31.11	907.45	766.46
Panel 17	181.91	31.89	899.13	793.23
Panel 18	182.86	32.87	941.01	815.78
Panel 19	182.48	32.99	869.18	810.27
Panel 20	182.86	28.42	882.12	698.81
Panel 21	183.42	28.42	972.86	698.81
Panel 22	186.90	55.6	2043.24	1386.63
Panel 23	185.41	57.35	2097.22	1430.75
Panel 24	185.44	57.29	2066.68	1431.64
Panel 25	185.54	56.82	2035.38	1416.71
Panel 26	186.76	56.57	2139.29	1412.66
Panel 27	187.19	57.18	2065.4	1422.64
Panel 28	186.93	55.61	2065.16	1393.46

3. CONCLUSIONS

The observations suggested that the forces are relatively high on the higher wind velocities on the solar mounts. The highest probability of the possible dislocations or the marked trouble zones in solar mount panel in the case of 25 m/s wind velocity with a possible normal force of 1550 N and a possible lift force of

4600 N approximately. The problematic zones in the entire farm are the last row of the structured mounts. In contrast, the shear layer formed on the solar mounts is probably high in the same panel numbers. This work investigated the wind effects on roof-mounted solar panels to reduce the overall construction costs. The new hexagon design seems to be doing well with the wind loads comparatively with the eight scenarios explained in the results.

4. AUTHORS BIOGRAPHY

Dr. Panga Surendra Reddy is a Lecturer in the Department of Technical Education at Government Polytechnic, Proddatur. He received his doctoral degree from KL University in April 2023 and has published six research papers in reputed journals. His research interests include renewable and alternative energy materials, nanomaterials, thin films, nanophotonics, computational physics, and solar energy optimization

REFERENCES:

1. Chung, K., Chang, K. and Chou, C., (2011) Wind loads on residential and large-scale solar collector models, J. Wind Eng. Ind. Aerodyne, vol.99, No. 59-64.
2. Aly M. Aly and Bitsuamlak, G., (2013) Aerodynamics of ground-mounted solar panels: Test model scale effects in Proc. of the 13th American Wind Eng. Conf.,
3. Hangan, H., (2010) A study of wind effects for solar power products panel mount system, Report BLWT-SS8-2010, Alan G. Davenport Wind Engineering Group. Pratt,
4. Bitsuamlak, G.T. Dagnew, A.K. and Erwin, J., (2010) Evaluation of wind loads on solar panel modules using CFD, in Proc. of The Fifth International Symposium on Computational Wind Engineering, Chapel Hill, North Carolina, USA May 23-27.
5. Radu, A. Axinte, E. and Theohari, C., (1986) Steady wind pressures on solar collectors on flat-roofed buildings, J. Wind Eng. Ind. Aerodyne., vol.23, No.249-258. SEAOC, 2013, Solar Photovoltaic Systems, Wind design for low-profile solar photovoltaic arrays on flat roofs.
6. Chung, K. Chang, K. Liu, Y., (2008) Reduction of wind uplift of a solar collector model, J. Wind Eng. Ind. Aerodyne., vol.96, No. 1294-1306.
7. Hangan, H., (2010) A study of wind effects for solar power products panel mount system, Report BLWT-SS8-2010, Alan G. Davenport Wind Engineering Group.
8. Shademan, M. and Hangan, H., (2009) Wind Loading on Solar Panels at Different Inclination Angles, in Proc. of 11th Americas Conference on Wind Engineering, San Juan, PVerto Rico.
9. M. Shademan, R.M. Barron, R. Balachandar, and H. Hangan., (2014) Numerical simulation of wind loading on ground-mounted solar panels at different flow configurations, Can. J. Civ. Eng. vol.41, No.728–738.
10. D. RoeleveldG, HailuA.S. FungD. NaylorT. YangA.K. Athienitis., (2015) Validation of Computational Fluid Dynamics (CFD) Model of a Building Integrated Photovoltaic/Thermal (BIPV/T) System, Energy Procedia, 78.No. 1901– 1906.
11. Hao Lu, Wenjun Zhao., (2019) Cfd prediction of dust pollution and impact on an isolated ground mounted solar photo voltaic system. Renewable energy.vol.131, No.829-840.
12. Mohammed, Gofran Chowdury, Dirk Goosseens, HansGoverde, Francky Catthoor., (2018) Experimental validated CFD simulations predicting wing effects on photo voltaic modules mounted on inclined surfaces. Sustainable Energy Technologies and assessments, vol.30, No.201-208.